International Journal of Concrete Structures and Materials

RESEARCH Open Access

Effect of Supplementary Cementitious Materials on Post-fire Performance of Concrete Columns

Yeokyeong Lee[1], Yeonju Chun[2], Venkatesh Kodur[1,3] and Hee Sun Kim[1*]

Abstract

This study evaluates the material behavior of heated concrete with varying supplementary cementitious material (SCM) contents and quantifies its effect on the post-fire performance of reinforced concrete (RC) columns. The novelty of this research lies in examining the influence of SCM content on the residual behavior of heated concrete and its application to RC columns exposed to fire. Concrete specimens were prepared with different mix ratios of fly ash and slag ranging from 0% to 30% of the total binder weight. Residual stress–strain responses were obtained by testing the specimens after exposure to elevated temperatures. These material properties were then incorporated into finite element (FE) models of full-scale RC columns. Thermo-mechanical coupled analyses and structural analyses were sequentially performed to predict the post-fire performance of the columns. The results indicate that the load-bearing capacity of fire-damaged columns cannot be explained solely by the material behaviors of concrete. Notably, the column containing concrete with 10% fly ash and 10% slag demonstrated greater residual load capacity than other models, despite having strength and elasticity not always higher compared to other concrete mixtures. Nonetheless, the residual strength ratio of the columns correlates with that of concrete in general. A comparison between structural and material behaviors indicates that the residual strength ratios of the columns align with those of concrete heated to 400–500 ℃.

Keywords Supplementary cementitious material, Fly ash, Blast furnace slag, Concrete column, Residual response, Post-fire performance

1 Introduction

In recent years, concrete mixed with supplementary cementitious materials (SCMs), such as fly ash and blast furnace slag, has been widely utilized worldwide. This is due to SCMs' ability to enhance the durability of concrete and simultaneously reduce carbon dioxide emissions by partially replacing cement. As the demand for SCMs grows in the concrete industry, research on their influence on concrete behavior under high-temperature conditions has intensified. Studies have demonstrated that replacing cement with SCMs improves fire endurance and compressive strength (Fan et al., 2019; Karahan, 2017; Lai et al., 2023; Lu et al., 2020; Ramzi & Hajiloo, 2023; Shumuye et al., 2021; Tanyildizi & Coskun, 2008). Additionally, SCMs enhance other

Journal information: ISSN 1976-0485 / eISSN 2234-1315.

*Correspondence:
Hee Sun Kim
hskim3@ewha.ac.kr
[1] Department of Architectural and Urban Systems Engineering, Ewha Womans University, 52, Ewhayeodae-gil, Seodaemun-gu, Seoul 03760, Republic of Korea
[2] Department of Construction Test & Certification, Korea Institute of Civil Engineering and Building Technology, 283, Goyang-daero, Ilsanseo-gu, Goyang-si, Gyeonggi-do 10223, Republic of Korea
[3] Department of Civil and Environmental Engineering, Michigan State University, East Lansing, MI 48824, USA

mechanical properties such as flexural capacity, splitting tensile resistance, and bending strength under high temperatures (Singh et al., 2023; Tanyildizi & Coskun, 2008; Zhang et al., 2015). Moreover, spalling was not observed at temperatures up to 350–450 ℃ (Cree et al., 2013) when SCMs were added to the concrete. These improvements are attributed to SCMs' ability to densify the C–S–H gel structure (Shumuye et al., 2021) and their self-healing properties during post-fire curing (Ming & Cao, 2020). Residual strength has been shown to improve in concretes exposed to temperatures of up to 400–450 ℃ (Cree et al., 2013; Li et al., 2012; Singh et al., 2023), while strength degradation occurs at temperatures exceeding 500 ℃ (Chun et al., 2023; Fan et al., 2019; Karahan, 2017; Lai et al., 2023; Ramzi & Hajiloo, 2023; Tanyildizi & Coskun, 2008). However, limited research has extended the understanding of the residual material behavior of SCM-incorporated concrete to the structural level.

To address this gap, studies have explored the post-fire performance of concrete structures incorporating SCMs. Concrete beams containing SCMs, such as fly ash and steel slag powder, generally exhibit equivalent post-fire performance in load–deflection response, crack pattern, and cutline stiffness. Moreover, they demonstrated improved energy dissipation capacity and resistance to initial cracking (Oktaviani et al., 2020; Zhang et al., 2025) compared to pure cement concrete beams. However, ductility and flexural capacity decreased significantly with increasing temperature and exposure time (Liu et al., 2024; Mathew & Joseph, 2018). In slabs, the addition of SCMs had a slightly adverse effect on compressive strength and deflection when exposed to high temperatures (Ghazy et al., 2022; Mussa et al., 2021).

The post-fire behavior of reinforced concrete (RC) columns depends on factors such as concrete strength (Ali et al., 2010; Eamon & Jensen, 2013; Pul et al., 2021; Tao & Yu, 2012), concrete type (Gernay et al., 2013; Kodur et al., 2013), fire exposure duration (Chen et al., 2009; Demir et al., 2020; Pul et al., 2021; Tao & Yu, 2012), and temperature (Eamon & Jensen, 2013). For instance, Khaliq and Kodur (2013) conducted an experimental study on high-strength concrete columns with and without fly ash to evaluate their post-fire behavior. The results showed that the fire resistance and thermal response of fly ash concrete columns were similar to those of pure cement concrete columns and the structural response was slightly better due to improved microstructure and enhanced tensile strength resulting from the addition of fly ash in concrete. Similarly, Mathews et al. (2022), examined self-compacting concrete columns incorporating fly ash and ground granulated blast furnace slag under varying fire exposure durations. Their findings revealed that slag-incorporated concrete columns exhibited superior residual strength and load-carrying capacity compared to the columns with fly ash. However, the above mentioned studies do not quantify the detailed extent to which SCM content influences the residual material properties of concrete and the post-fire performance of structural members.

To address this limitation, the present study investigates the effects of SCM content in concrete on the post-fire performance of RC columns by analyzing both material and structural behaviors. Material tests were conducted on concrete with varying fly ash-to-slag ratios to obtain residual stress–strain relationships after exposure to temperatures of 200 ℃, 500 ℃, and 800 ℃ for 3 h. The test results of stress–strain curves were employed as material properties in finite element (FE) models of full-scale RC columns to predict their structural response after fire exposure. Thermo-mechanical coupled analyses were performed to simulate asymmetric heating and eccentric axial loading applied to the RC columns. Subsequently, structural analyses were conducted on fire-damaged columns considering temperature distributions and deformed shapes. The load–displacement responses of columns with varying SCM contents were analyzed, providing new insights into the residual material behavior of SCM-incorporated concretes and the post-fire performance of RC columns.

2 Study Methodology

The methodology adopted in this study comprises material-level tests on concrete specimens with varying SCM contents to determine the residual mechanical properties of the concrete, and a series of FE-based numerical simulations to evaluate the post-fire performance of RC columns with varying SCM contents.

2.1 Material-Level Test on Concrete with Different SCM Content

2.1.1 Concrete Specimen Preparation

To investigate the residual material behavior of the SCM-incorporated concrete after exposure to high temperatures, heating and compressive strength tests were conducted on cylindrical concrete specimens. The batch mix proportions of concrete in Table 1 were designed with varying fly ash and blast furnace slag contents, ranging from 0% to 30% of the total binder weight. Materials, including fly ash and slag, were supplied by Aju Corporation (South Korea) and Total PC (South Korea). The mix ratios of the fly ash-slag were varied as follows: 0–0% (F0-S0) for pure cement concrete, 20–0% (F20-S0) for fly ash composite concrete, 5–15% (F5-S15), 10–10% (F10-S10), 15–5% (F15-S5) for typical ternary blended concrete, and 30–10% (LF30-S10) for low cement concrete. All specimens targeted a

Table 1 Mix proportions of the concrete

Specimen	W/B	Water	Cement	Fly ash	Slag	Fine aggregate	Coarse aggregate	Superplasticizer	PP fiber
	%	kg/m^3							Vol%
F0-S0	26	157	604	0	0	681	921	6.04	0.15
F20-S0			484	120	0	662	895		
F5-S15				30	90	666	909		
F10-S10				60	60				
F15-S5				90	30				
LF30-S10	28	140	300	150	50	611	1063		

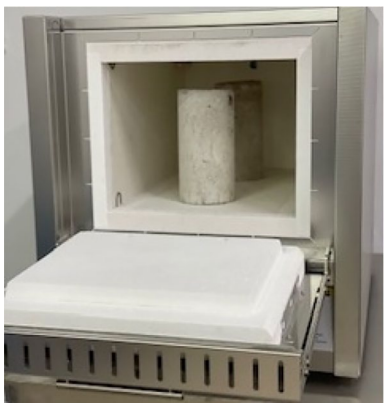

Fig. 1 Heating test of the concrete specimen

Fig. 2 Compressive strength test after exposure to heating

compressive strength of 60 MPa. A superplasticizer was added to the concrete mixtures to enhance workability, and polypropylene (PP) fibers (length: 6 mm) were included to prevent spalling during heating tests. Specimen fabrication of concrete specimens followed KS F 2403 standard (KS F 2403 2019), and specimens were cured in water after demolding. The 28-day compressive strengths of the unheated specimens were as follows: F0-S0 (67.1 MPa), F20-S0 (64.7 MPa), F5-S15 (65.1 MPa), F10-S10 (67.2 MPa), F15-S5 (69.5 MPa), and LF30-S10 (61.8 MPa).

2.1.2 Heating Test

To prevent spalling and delayed heat propagation caused by excessive moisture content, specimens were air-cured for over 90 days before heating (Li et al., 2017; Lin et al., 2011). They were then heated at 200 ℃, 500 ℃, and 800 ℃ for 3 h in a muffle furnace (Nabertherm, Germany), as depicted in Fig. 1. The heating duration was determined based on an analytical study that confirmed uniform temperature distribution within the concrete specimens. The temperature increase rate was controlled to not exceed that of the ISO 834 standard fire curve (approximately 8 ℃/min), as exceeding this rate could lead to concrete spalling during heating. After heating, the specimens were slowly removed from the furnace to minimize thermal shock and were sufficiently air-cooled to mitigate changes in residual mechanical properties due to the cooling method (Akbulut et al., 2024).

2.1.3 Compressive Strength Test

Residual compressive strengths were measured one day after heating. Loads were applied following ASTM C39M until the specimens failed. A compressor meter was used to measure strain during loading (Fig. 2). Data, including loads and strains, were recorded every second using a data logger (Tokyo Measuring Instruments Lab., Japan). The procedure was repeated two or three times per variable to ensure consistency, and the average values were reported.

Table 2 presents the maximum strengths and elastic moduli of the concrete specimens obtained from the compressive strength tests. The strengths at 200 ℃ of F20-S0 and LF30-S10 were higher than unheated concrete strengths. This phenomenon is likely attributed to the self-healing properties of SCMs, activated during post-fire curing (Fan et al., 2019; Ming & Cao, 2020; Tanyildizi & Coskun, 2008). Significant reductions in strength and elasticity were observed in the specimens after exposure to temperatures of 500 ℃ and above. Interestingly, ternary blended concrete specimens (F5-S15, F10-S10, and

Table 2 Compressive strengths and elastic moduli of the concrete specimens

	Specimen	Unheated	Heated temperature		
		20 ℃	200 ℃	500 ℃	800 ℃
Compressive strength [MPa]	F0-S0	67.1	65.5	39.9	9.9
	F20-S0	64.7	71.5	37.8	12.7
	F5-S15	65.1	56.4	32.8	13.3
	F10-S10	67.2	63.5	37.7	13.4
	F15-S5	69.5	63.4	32.6	11.6
	LF30-S10	61.8	69.3	38.5	10.5
Elastic modulus [GPa]	F0-S0	39.0	17.4	3.8	0.5
	F20-S0	37.6	19.0	3.5	0.7
	F5-S15	37.7	26.2	6.3	1.5
	F10-S10	30.3	24.9	9.4	2.0
	F15-S5	37.8	23.7	6.6	1.6
	LF30-S10	31.5	14.9	4.6	0.6

F15-S5) exhibited higher elastic moduli at 200 ℃, 500 ℃, and 800 ℃ compared to others, despite having similar or lower elastic moduli at 20 ℃. However, determining whether specific specimens consistently exhibit superior residual material properties remains challenging. Further investigation into the chemical reactions between SCMs at elevated temperatures is necessary to explain the reason for variations in material characteristics associated with different SCM mix ratios. To better understand the relationship between residual ratios at the material and structural levels, Table 5 lists the percentages of concrete strength after exposure to high temperatures compared to its strength at room temperature at material and structural levels.

2.2 Analytical Study for the Column Evaluation

An FE analytical study was conducted to examine the effect of varying SCM mix ratios on the post-fire performance of full-scale RC columns. The analytical method, outlined in the flowchart (Fig. 3), consisted of two sequential analyses: thermo-mechanical coupled analysis and structural analysis. The thermo-mechanical coupled analysis was performed to predict the behavior of RC columns during heating, including deformed shapes and temperature distributions. These results were then

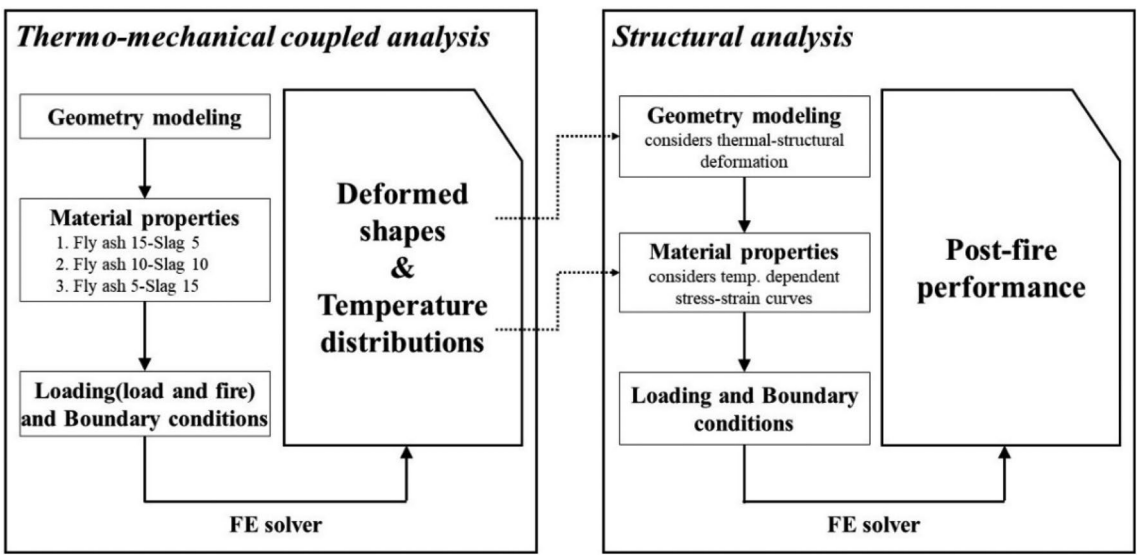

Fig. 3 Flowchart of the FE analytical approach

used to generate damaged column models, which served as input for the structural analysis. The structural analysis evaluated the residual strength and overall performance of the columns after exposure to elevated temperatures. Finally, the post-fire performance of the damaged columns, considering different SCM content, was obtained. The overall modeling methodology adopted in this paper is based on our previously undertaken studies. Especially, Lee and Kim (2023) reported the effect of thermal deformations and geometrical nonlinearity on predictions of post-fire performance of RC walls. Moreover, the material test simulation with implementation of material models obtained from the tests agreed well with the test results. Therefore, this study adopted the developed modeling methods to RC column models. The detailed analytical approaches will be described in the following subsections.

2.2.1 Thermo-Mechanical Coupled Analysis

To investigate under real-life conditions, the column details were chosen from a typical structural plan of a high-rise building (Ryu, 2020). As illustrated in Fig. 4a, the initial dimensions of the column were 450 mm × 750 mm × 3000 mm (width × depth × height), with longitudinal reinforcement comprising 8-D19 steel bars (eight deformed steel bars, 19 mm in diameter) and transverse reinforcement of D13@300 stirrups (13 mm diameter, spaced at 300-mm intervals). The FE model was generated and analyzed using ABAQUS version 2020 (Dassault Systems, Velizy-Villacoublay, France). Concrete was modeled with 3D continuum thermally coupled brick elements featuring reduced integration point (C3D8RT), while steel reinforcements were modeled using 3D-coupled temperature-displacement truss elements (T3D2T). The element size was set at 30 mm to optimize computational efficiency and facilitate temperature profile readings. A perfect bond was assumed between the concrete and reinforcing steel.

The mechanical behaviors of concrete with different SCM mix ratios were modeled based on stress–strain relationships obtained from material-level tests. However, for F0-S0 and F20-S0, due to experimental limitations, Eurocode 2 was used to derive stress–strain relations as ratios of stress to maximum strength at various temperatures; stress values were based on the experimental results, while stress–strain relations were calculated using Eurocode 2. Thermal material properties, such as conductivity and heat capacity, were assumed to align with those of concrete containing only fly ash (Kodur et al., 2004). The effect of varying SCM contents on thermal properties was disregarded based on the previous findings that suggest negligible influence (Kodur & Khaliq, 2011). For steel, both mechanical and thermal material properties were obtained from previously reported data (Chun et al., 2022).

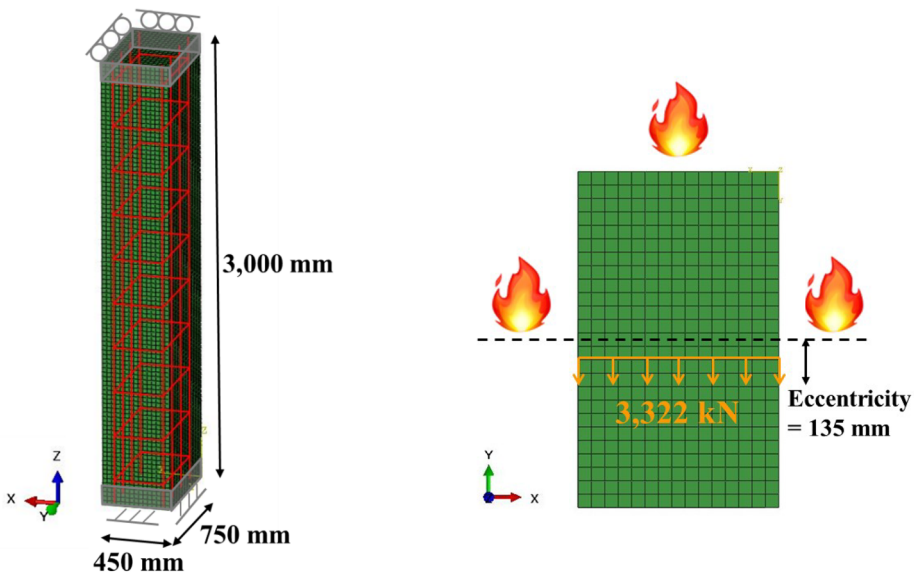

(a) Column dimensions and boundary conditions.

(b) Fire and loading prescriptions.

Fig. 4 Details of the FE column model for the thermo-mechanical coupled analysis. **a** Column dimensions and boundary conditions. **b** Fire and loading prescriptions

Heating temperatures were applied exclusively to the three side-surfaces of the column following the ISO 834 time–temperature curves. This approach reflects the location of the column in the middle of an external wall, where one side faces the exterior and the other three sides are exposed to interior conditions. This configuration not only adheres to the geometry of the column as specified in the structural plan of a high-rise building (Ryu, 2020), but also accounts for a realistic fire scenario that results in asymmetric fire exposure to the column. The base of the column, with a height of 120 mm, was fixed in all translational directions, assuming that the column was embedded in a slab. The upper part, also 120 mm in height, was restrained only in the horizontal directions. Prior to heating, a load of 3322 kN—equivalent to approximately 22.3% of the nominal axial loading capacity—was applied with an eccentricity of 135 mm. This eccentricity corresponds to 0.3 times the column width and half of the balanced eccentricity. The magnitude of the applied load was determined based on the column's location and building purpose, while the eccentricity was determined to amplify the effects of asymmetry on the cross-sectional properties of the column, as shown in Fig. 4b. The mechanical load was kept constant throughout the 2-h heating period. For the nonlinear analysis, convergence control was employed. The maximum time interval was set to correspond to a temperature increase of 1 ℃, while the minimum time interval was set to 1/100,000 of the maximum interval.

After heating, the concrete temperatures within the column ranged from 20 ℃ to 1050 ℃, with the maximum temperature of the steel reinforcement reaching 556 ℃. Because the influence of the SCM content on the thermal material properties was disregarded in the material modeling, the representative temperature distributions for the concrete and steel reinforcements are illustrated in Fig. 5a and b, respectively. Due to the combined effects of heating and loading, the columns exhibited both lateral and axial deformations after the thermo-mechanical coupled analyses. Fig. 6 presents the von Mises stress and equivalent plastic strain distributions on the deformed shapes of the column, which are nearly identical across all models. The maximum stress in the concrete and the yield strain in the steel were observed at the location of eccentric loading. Additionally, steel near the fixed region failed, particularly at the corners of the heated side surfaces. Asymmetric heating and eccentric loading caused lateral deformations of approximately 4.8 mm in all column models. In the axial direction, the columns expanded due to thermal deformation, which dominated the effects of mechanical loading (22.3% of the nominal axial loading capacity). Axial deformations in the z-direction measured 11.5, 11.1, 11.0, 10.8, 11.2, and 10.7 mm for columns with F0-S0, F20-S0, F5-S15, F10-S10, F15-S5, and LF30-S10, respectively. Table 3 lists the natural frequencies at 1st ~ 6th modes for fire-damaged column models. These frequencies, which ranged from 0.04435 to 0.54743, are attributed to the deformations caused by fire and structural loadings (Akbulut et al., 2021, Altunisik et al., 2022). Although the simulated columns displayed similar temperature, stress, and strain contours regardless of variations in SCM content, their axial deformations differed.

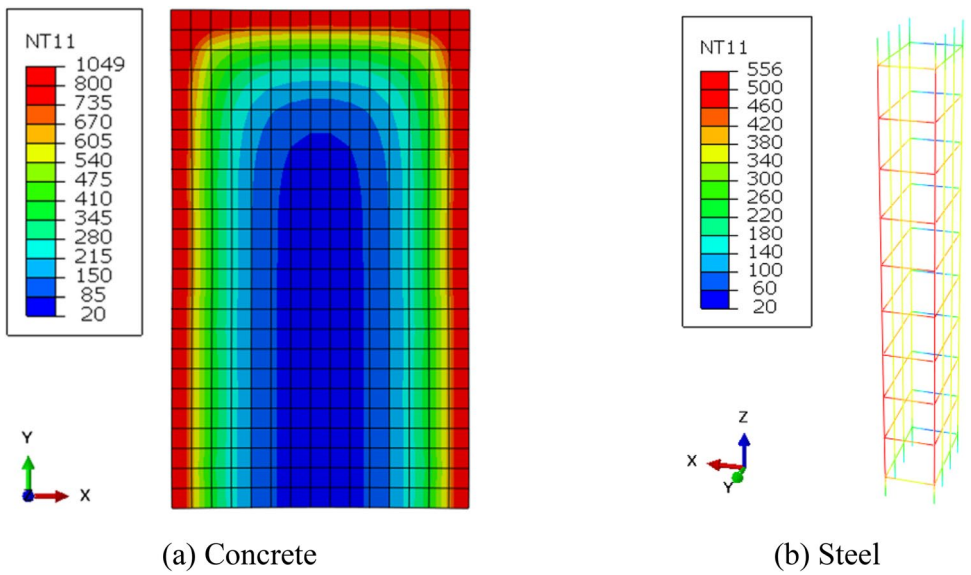

Fig. 5 Temperature distributions of the column after 2 h of heating. **a** Concrete. **b** Steel

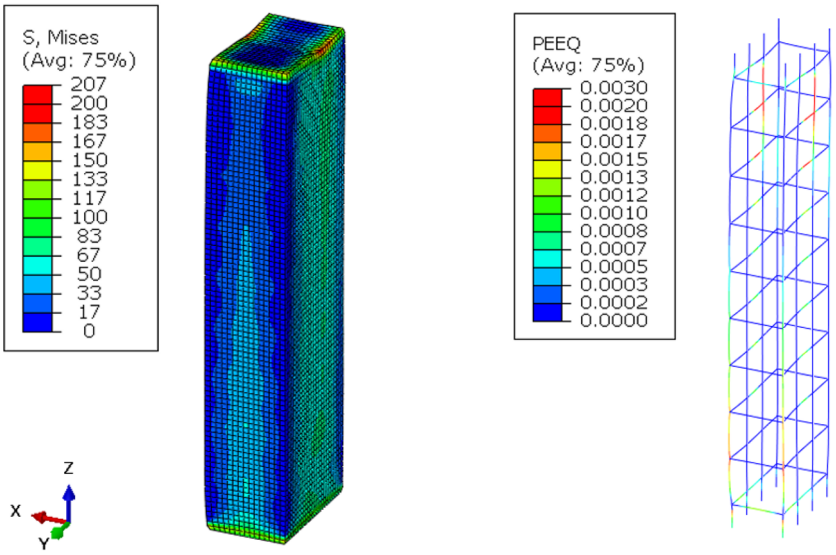

(a) Von Mises stress distributions of concrete within the effective length (2760 mm).

(b) Equivalent plastic strain distributions of the steel.

Fig. 6 Deformed shapes of the column after thermal and mechanical loadings; the deformation scale factor is 10. **a** Von Mises stress distributions of concrete within the effective length (2760 mm). **b** Equivalent plastic strain distributions of the steel

Table 3 Comparison of the natural frequencies of the fire-damaged column

Mode	Natural frequency [Hz]						Standard deviation
	F0-S0	F20-S0	F5-S15	F10-S10	F15-S5	LF30-S10	
1	0.4835	0.4953	0.5618	0.5806	0.5549	0.4814	0.04435
2	0.9869	1.0046	1.1266	1.1131	1.1084	0.9335	0.08093
3	2.5330	2.6020	3.0045	3.0855	2.9603	2.4900	0.26572
4	2.8588	2.9274	3.3217	3.4120	3.2792	2.8279	0.26096
5	5.0721	5.1614	5.7942	5.7028	5.6991	4.7758	0.42055
6	6.8464	6.9460	7.7534	7.5127	7.6181	6.3424	0.54743

Notably, the column with F0-S0 showed the largest deformation due to having the highest elastic modulus reduction of concrete.

2.2.2 Structural Analysis

The FE models for the structural analysis were generated based on the deformed geometries of the columns obtained from the previous thermo-mechanical coupled analysis. The nodal coordinates of each element were extracted from the output data of the thermo-mechanical coupled analyses, and the elements for the structural analysis were generated while preserving the node numbering and meshing order. However, these models cannot be considered fully coupled, as the cracks caused by thermal and structural loadings were not modeled, and neither temperature increases nor fracture mechanisms were applied to the columns. A 3D continuum brick element with a reduced integration point (C3D8R) was used for the concrete, while 3D truss elements (T3D2) were employed for the steel reinforcement.

The temperature-dependent residual material properties of the concrete were assigned to respective parts based on the temperature distributions obtained from the thermo-mechanical coupled analyses. To enhance computational efficiency, the material properties were assigned to the parts with intervals of 100 ℃–200 ℃, calculated using the average temperature within each mesh. For columns F0-S0 and F20-S0, which lacked experimentally derived stress–strain relationships,

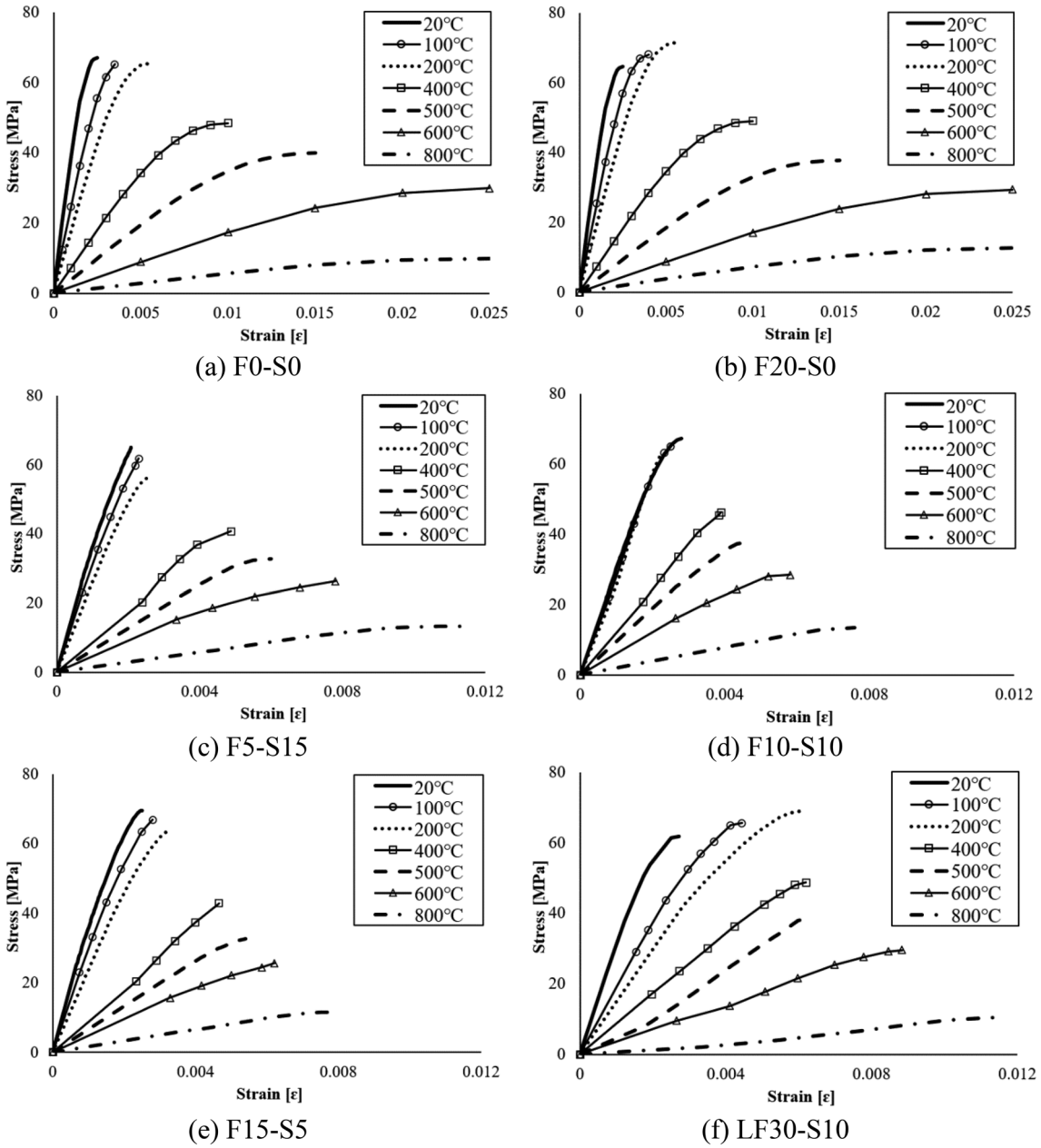

Fig. 7 Material models of concrete at elevated temperatures according to the SCM content

the material properties were adopted from Eurocode 2 and the measured compressive strengths (Fig. 7a and b). In contrast, the material models for F5-S15, F10-S10, F15-S5, and LF30-S10 were based on the test results of concrete specimens at 200 ℃, 500 ℃, and 800 ℃. For temperatures between these points, linear interpolations were used to determine the properties (Fig. 7c–f). For the fire-damaged steel reinforcement, the stress–strain curves reported in prior study by Chun et al. (2022) were adopted.

The boundary conditions and constraints between the concrete and steel reinforcement were similar to those used in the thermo-mechanical coupled analysis. Structural loads were incrementally applied until the analysis terminated due to numerical instability. The structural analyses accounted for both material and geometrical nonlinearities. Additionally, the Riks method was employed to capture buckling behavior, considering the high aspect ratio and slenderness of the columns.

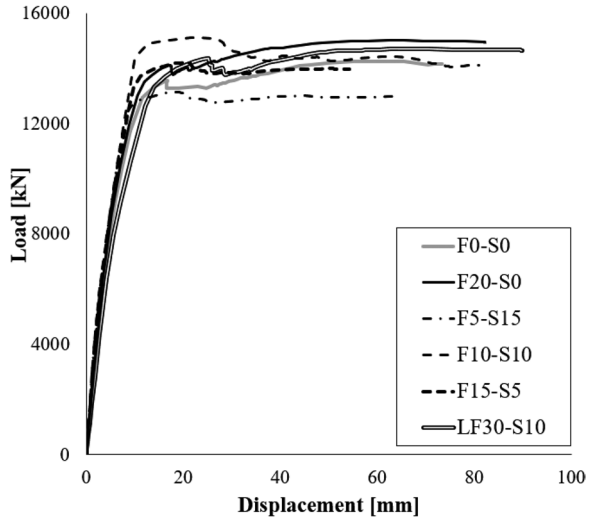

Fig. 8 Load–displacement response of the columns from the structural analyses

3 Results and Discussion

3.1 Load–Displacement Response

Fig. 8 illustrates the load–displacement responses predicted from the simulations of different columns. The initial stiffness values are nearly identical across all models. A load decrease is observed at displacements of 20–23 mm, which allows the strain energy of the columns to be released. The peak points of the load–displacement curves occurred earlier in the ternary blended concrete column models (F5-S15, F10-S10, and F15-S5), whereas in the other columns, these points were observed even after 60 mm of displacement. As a result, the maximum loads for the columns, ranked in descending order, are as follows: F10-S10 (15,107 kN), F20-S0 (15,014 kN), LF30-S10 (14,710 kN), F0-S0 (14,258 kN), F15-S5 (14,207 kN), and F5-S15 (13,136 kN).

The load–displacement curves from the structural analyses reveal that the post-fire performance of the concrete columns cannot be explained solely by the material properties of the concrete. The column model of F10-S10 exhibits the highest maximum load, as shown in Fig. 8. However, the strength and elasticity of the concrete in F10-S10 are not significantly higher than those of other models, both at room temperature and after exposure to high temperatures (Table 2). Although the residual concrete strength and elastic modulus at 800 ℃ are the highest in F10-S10, this ranking does not align with the maximum load-bearing capacities of the concrete columns. Therefore, numerical analysis or experimental investigations at the structural level are necessary to accurately assess the load capacity of fire-damaged columns.

Table 4 Comparison of the load capacity of the fire-damaged column

Specimen	Load-bearing capacity [kN]		Ratio of A/B [%]
	Predicted from the FE analysis (A)	Calculated from 500 ℃ isotherm method (B)	
F0-S0	14258	14053	101.4
F20-S0	15014	13588	110.5
F5-S15	13136	13666	96.1
F10-S10	15107	14072	107.4
F15-S5	14207	14517	97.8
LF30-S10	14710	13027	112.9

Furthermore, these results indicate that the 500 ℃ isotherm method, a simplified calculation method proposed by Eurocode 2, may not be suitable for evaluating the post-fire performance of columns made with SCM-incorporated concrete. The 500 ℃ isotherm method assumes that damaged concrete exposed to temperatures exceeding 500 ℃ does not contribute to the load-bearing capacity of the member, while the remaining concrete cross-section (below 500 ℃) retains its initial strength and elastic modulus. Table 4 compares the maximum loads of the column calculated using the 500 ℃ isotherm method with the results from the FE analysis in this study. The differences between the predictions from the FE analysis and the calculation from the 500 ℃ isotherm method are the smallest in the case of F0-S0 (pure cement concrete) as 1.4%, and largest for LF30-S10 (low cement concrete) as 12.9%. This discrepancy arises because the concrete strength at room temperature governs the load capacity of the column in 500 ℃ isotherm method, where the same residual cross-sections is assumed regardless of SCM content. Consequently, further research is required to determine the applicability of the 500 ℃ isotherm method for evaluating the structural performance of members made with SCM-incorporated concrete considering diverse material and structural conditions.

3.2 Residual Strength Ratio

Table 5 presents the ratios of the compressive strengths of heated concrete specimens to those of unheated specimens (at 20 ℃) and the ratios of the maximum loads of fire-damaged column models to those of control models, which were subjected only to eccentric loading without heating. The results provides a relationship between the residual strength ratio of the columns at the structural level and that of the concrete at the material level. Columns F20-S0, F10-S10, and LF30-S10 exhibit higher residual strength ratios (over 60%) compared to

Table 5 Residual strength ratios at the material and structural levels [%]

Specimen	Material level			Structural level
	Heated temperatures of the concrete			Column exposed to ISO-834 for 2 h
	200 ℃	500 ℃	800 ℃	
F0-S0	97.6	59.5	14.8	59.5
F20-S0	110.5	58.4	19.6	65.8
F5-S15	86.6	50.4	20.4	57.7
F10-S10	94.5	56.1	19.9	64.3
F15-S5	91.2	46.9	17.4	58.3
LF30-S10	112.1	62.3	17.0	66.9

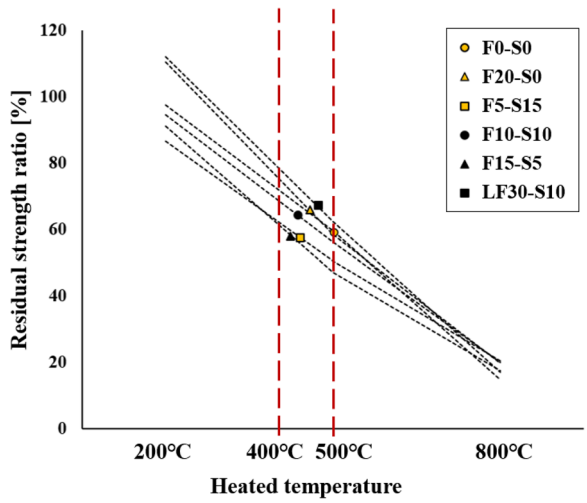

Fig. 9 Estimated point where the residual strength ratios at the material and structural levels are matched (black dashed lines: results from material studies)

other models, consistent with mostly higher residual strength ratios of their corresponding concretes at the material level. Fig. 9 illustrates the estimated points where the residual strength ratios of the concrete specimens and columns align. For the pure cement concrete model (F0-S0), the marking point is at 500 ℃ because its residual strength ratio at the column level (59.5%) matches the residual strength ratio of the concrete specimens heated with 500 ℃. For the SCM-mixed concrete models, the temperatures matching residual strength ratios of concrete specimens were determined by linear interpolation between 200 ℃ and 500 ℃. The matching temperatures for F20-S0, F5-S15, F10-S10, F15-S5, and LF30-S10 were found to be 457.39 ℃, 439.50 ℃, 435.94 ℃, 422.80 ℃, and 472.29 ℃, respectively. These results highlight the necessity of considering the overall residual strength ratios of concrete after exposure to high temperature, especially within the 400 ℃–500 ℃ range, when evaluating the residual strength ratio of columns.

When comparing F0-S0 and LF30-S10, it is found that the replacement of cement in concrete affects to the residual strength ratios and post-fire performance of RC columns. As shown in Table 1, the weight of cement used in F0-S0 is approximately double that in LF30-S10. Even though the concrete strength of F0-S0 at ambient conditions (67.1 MPa) is higher than that of LF30-S10 (61.8 MPa), the maximum load capacities of the fire-damaged columns are 14,258 kN for F0-S0 and 14,710 kN for LF30-S10. Furthermore, the residual strength ratio of the column with LF30-S10 (66.9%) is significantly higher than that of the column with F0-S0 (59.5%). This indicates that the replacement of cement with SCMs likely enhanced the residual load capacity of the columns after fire exposure.

4 Conclusion

This study investigated the effects of SCM content on the residual material behaviors of concrete exposed to high temperatures and the post-fire performance of full-scale RC columns. Experimental tests, including heating and compressive strength tests were conducted on concrete specimens with six different mix proportions of fly ash and blast furnace slag: 0% (F0-S0), 20–0% (F20-S0), 5–15% (F5-S15), 10–10% (F10-S10), 15–5% (F15-S5), and 30–10% (LF30-S10). FE-based analytical methods were also used to predict the residual load-bearing capacity and structural response of columns incorporating SCM-mixed concrete. Further research is recommended to expand the applicability of the findings toward wide ranges of parameters including the post-fire behavior of ultra-high-performance-concrete or zero-cement concrete, the effect of alternative SCM types (e.g., silica fume) on residual concrete strength at high temperatures, and the effect of SCMs on the shear and tensile behaviors of concrete. The key findings of this study are as follows:

(1) Residual material behavior of concrete is influenced by SCM content. Among specimens with a 20% replacement of cement, residual strength, elasticity, and residual strength ratio varied based on the fly ash–slag content. However, no single mix consistently demonstrated superior residual behavior after exposure to high temperatures.
(2) The column with the F10-S10 mix exhibited the highest maximum load capacity, even though the strength and elasticity of the F10-S10 concrete were not the highest among the tested mixes. This highlights the necessity of conducting numerical analyses or full-scale experiments at structural

level, as post-fire performance of column cannot be determined solely based on the material behaviors of the concrete.

(3) The LF30-S10 column model, which was a ternary blended with low cement content, showed the largest discrepancy between predictions from the FE analysis and results calculated using the 500 ℃ isotherm method. In contrast, the F0-S0 column model (pure cement concrete) exhibited the smallest discrepancy. This suggests that the 500 ℃ isotherm method may not adequately account for the effects of SCM content in concrete on post-fire performance of RC column.

(4) Mixes such as F20-S0, F10-S10, and LF30-S10 exhibited relatively higher residual strength ratios not only at the material level, but also in column. The ratio of the maximum load of the fire-damaged column to that of the unheated column is closely linked to the residual strength ratio of the concrete. Evaluating residual strength ratios of concrete exposed to high temperature—particularly in the 400–500 ℃ range—is important when predicting the post-fire residual strength of the columns.

Acknowledgements
The authors are grateful for the help of Ha-Eun Min, the master's course in the Department of Architectural and Urban Systems Engineering, Ewha Womans University, in conducting experiments.

Author contributions
Yeokyeong Lee: data curation, writing—original draft, writing—review and editing. Yeonju Chun: data curation, investigation. Venkatesh Kodur: methodology, writing—review and editing. Hee Sun Kim: conceptualization, supervision, writing—review and editing.

Funding
The work was supported by Basic Science Research Program funded by the National Research Foundation of Korea (NRF) [NRF-2021R1F1A1051300].

Availability of data and materials
All data generated of analyzed during this study are included in this published article.

Declarations

Ethics approval and consent to participate
Not applicable.

Consent for publication
Not applicable.

Competing interests
The authors declare that they have no known competing interests.

Received: 19 September 2024 Accepted: 1 March 2025
Published online: 04 May 2025

References

Akbulut, Y. E., Altunisik, A. C., Basaga, H. B., Mostofi, S., Mosallam, A., & Wafa, L. F. (2021). Numerical investigation on dynamic characteristics changes of RC columns and frames under elevated temperature. *Computers and Concrete, 28*(2), 149–187. https://doi.org/10.12989/cac.2021.28.2.149

Akbulut, Y. E., Nayır, S., Altunışık, A. C., Kahya, V., Sünnetci, M. O., & Ersoy, H. (2024). Experimental assessment of FRP repairing in concrete cylinders exposed high temperatures. *Case Studies in Construction Materials, 21*, e03656. https://doi.org/10.1016/j.cscm.2024.e03656

Ali, F., Nadjai, A., & Choi, S. (2010). Numerical and experimental investigation of the behavior of high strength concrete columns in fire. *Engineering Structures, 32*(5), 1236–1243. https://doi.org/10.1016/j.engstruct.2009.12.049

Altunişik, A. C., Akbulut, Y. E., Başağa, H. B., Mostofi, S., Mosallam, A., & Wafa, L. F. (2022). Experimental investigation on dynamic characteristics changes of fire exposed reinforced concrete and steel members. *Fire Technology, 58*(3), 1169–1208. https://doi.org/10.1007/s10694-021-01189-9

Chen, Y. H., Chang, Y. F., Yao, G. C., & Sheu, M. S. (2009). Experimental research on post-fire behaviour of reinforced concrete columns. *Fire Safety Journal, 44*(5), 741–748. https://doi.org/10.1016/j.firesaf.2009.02.004

Chun, Y., Kwon, J., Kim, J., Son, H., Heo, S., Cho, S., & Kim, H. (2023). Experimental investigation of the strength of fire-damaged concrete depending on admixture contents. *Construction and Building Materials, 378*, 131143. https://doi.org/10.1016/j.conbuildmat.2023.131143

Chun, Y., Ryu, E., Lee, Y., Kim, H., & Shin, Y. (2022). Experimental and analytical studies for the size effect on the axial strength of high-strength concrete walls with various fire-damaged areas. *International Journal of Concrete Structures and Materials, 16*(1), 32. https://doi.org/10.1186/s40069-022-00519-7

Cree, D., Green, M., & Noumowé, A. (2013). Residual strength of concrete containing recycled materials after exposure to fire: A review. *Construction and Building Materials, 45*, 208–223. https://doi.org/10.1016/j.conbuildmat.2013.04.005

Demir, U., Goksu, C., Unal, G., Green, M., & Ilki, A. (2020). Effect of fire damage on seismic behavior of cast-in-place reinforced concrete columns. *Journal of Structural Engineering, 146*(11), 04020232. https://doi.org/10.1061/(ASCE)ST.1943-541X.000279

Eamon, C. D., & Jensen, E. (2013). Reliability analysis of reinforced concrete columns exposed to fire. *Fire Safety Journal, 62*, 221–229. https://doi.org/10.1016/j.firesaf.2013.10.002

Fan, K., Li, D., Damrongwiriyanupap, N., & Li, L. Y. (2019). Compressive stress–strain relationship for fly ash concrete under thermal steady state. *Cement and Concrete Composites, 104*, 103371. https://doi.org/10.1016/j.cemconcomp.2019.103371

Gernay, T., & Salah Dimia, M. (2013). Structural behaviour of concrete columns under natural fires. *Engineering Computations, 30*(6), 854–872.

Ghazy, M. F., Abd Elaty, M. A., & Zalhaf, N. M. (2022). Modeling the performance of reinforced concrete slabs cast with high-performance concrete under fire. *Innovative Infrastructure Solutions, 7*(2), 171. https://doi.org/10.1007/s41062-022-00770-7

Karahan, O. (2017). Transport properties of high volume fly ash or slag concrete exposed to high temperature. *Construction and Building Materials, 152*, 898–906. https://doi.org/10.1016/j.conbuildmat.2017.07.051

Khaliq, W., & Kodur, V. (2013). Behavior of high strength fly ash concrete columns under fire conditions. *Materials and Structures, 46*, 857–867. https://doi.org/10.1617/s11527-012-9938-7

Kodur, V., & Khaliq, W. (2011). Effect of temperature on thermal properties of different types of high-strength concrete. *Journal of Materials in Civil Engineering, 23*(6), 793–801. https://doi.org/10.1061/(ASCE)MT.1943-5533.0000225

Kodur, V. K. R., Raut, N. K., Mao, X. Y., & Khaliq, W. (2013). Simplified approach for evaluating residual strength of fire-exposed reinforced concrete columns. *Materials and Structures, 46*, 2059–2075. https://doi.org/10.1617/s11527-013-0036-2

Kodur, V. K. R., Wang, T. C., & Cheng, F. P. (2004). Predicting the fire resistance behaviour of high strength concrete columns. *Cement and Concrete Composites, 26*(2), 141–153. https://doi.org/10.1016/S0958-9465(03)00089-1

KS F 2403. (2019). *Standard test method for making concrete specimens*. Korean Standards.

Lai, M. H., Chen, Z. H., Cui, J., Zhong, J. P., Wu, Z. R., & Ho, J. C. M. (2023). Enhancing the post-fire behavior of steel slag normal-strength concrete by adding SCM. *Construction and Building Materials, 398*, 132336. https://doi.org/10.1016/j.conbuildmat.2023.132336

Lee, C. E., & Kim, H. (2023). Analytical studies for prediction of residual strength of fire-damaged concrete walls considering geometric nonlinearity. *Proceedings of the Korea Concrete Institute, 35*(2), 213–214.

Li, L., Jia, P., Dong, J., Shi, L., Zhang, G., & Wang, Q. (2017). Effects of cement dosage and cooling regimes on the compressive strength of concrete after post-fire-curing from 800 ℃. *Construction and Building Materials, 142*, 208–220. https://doi.org/10.1016/j.conbuildmat.2017.03.053

Li, Q., Li, Z., & Yuan, G. (2012). Effects of elevated temperatures on properties of concrete containing ground granulated blast furnace slag as cementitious material. *Construction and Building Materials, 35*, 687–692. https://doi.org/10.1016/j.conbuildmat.2012.04.103

Lin, Y., Hsiao, C., Yang, H., & Lin, Y. F. (2011). The effect of post-fire-curing on strength–velocity relationship for nondestructive assessment of fire-damaged concrete strength. *Fire Safety Journal, 46*(4), 178–185. https://doi.org/10.1016/j.firesaf.2011.01.006

Liu, Y., Du, P., Tan, K. H., Du, Y., Su, J., & Shi, C. (2024). Experimental and analytical studies on residual flexural behaviour of reinforced alkali-activated slag-based concrete beams after exposure to fire. *Engineering Structures, 298*, 117035. https://doi.org/10.1016/j.engstruct.2023.117035

Lu, D., Tang, Z., Zhang, L., Zhou, J., Gong, Y., Tian, Y., & Zhong, J. (2020). Effects of combined usage of supplementary cementitious materials on the thermal properties and microstructure of high-performance concrete at high temperatures. *Materials, 13*(8), 1833. https://doi.org/10.3390/ma13081833

Mathew, G., & Joseph, B. (2018). Flexural behaviour of geopolymer concrete beams exposed to elevated temperatures. *Journal of Building Engineering, 15*, 311–317. https://doi.org/10.1016/j.jobe.2017.09.009

Mathews, M. E., Kiran, T., Anand, N., Lubloy, E., Naser, M. Z., & Arulraj, G. P. (2022). Effect of protective coating on axial resistance and residual capacity of self-compacting concrete columns exposed to standard fire. *Engineering Structures, 264*, 114444. https://doi.org/10.1016/j.engstruct.2022.114444

Ming, X., & Cao, M. (2020). Development of eco-efficient cementitious composites with high fire resistance and self-healing abilities-a review. *Resources, Conservation and Recycling, 162*, 105017. https://doi.org/10.1016/j.resconrec.2020.105017

Mussa, M. H., Radzi, N. A. M., Hamid, R., & Mutalib, A. A. (2021). Fire resistance of high-volume fly ash RC slab inclusion with nano-silica. *Materials, 14*(12), 3311. https://doi.org/10.3390/ma14123311

Oktaviani, W. N., Tambusay, A., Komara, I., Sutrisno, W., Faimun, F., & Suprobo, P. (2020). Flexural behaviour of a reinforced concrete beam blended with fly ash as supplementary material. *IOP Conference Series Earth and Environmental Science, 506*(1), 012042. https://doi.org/10.1088/1755-1315/506/1/012042

Pul, S., Atasoy, A., Senturk, M., & Hajirasouliha, I. (2021). Structural performance of reinforced concrete columns subjected to high-temperature and axial loading under different heating-cooling scenarios. *Journal of Building Engineering, 42*, 102477. https://doi.org/10.1016/j.jobe.2021.102477

Ramzi, S., & Hajiloo, H. (2023). The effects of supplementary cementitious materials (SCMs) on the residual mechanical properties of concrete after exposure to high temperatures. *Buildings, 13*(1), 103. https://doi.org/10.3390/buildings13010103

Ryu, E. (2020). Post-fire structural performance of high strength concrete walls and columns. *Doctoral dissertation, Ph. D. dissertation, Ewha Womans University, Korea*.

Shumuye, E. D., Zhao, J., & Wang, Z. (2021). Effect of the curing condition and high-temperature exposure on ground-granulated blast-furnace slag cement concrete. *International Journal of Concrete Structures and Materials, 15*, 1–20. https://doi.org/10.1186/s40069-020-00437-6

Singh, H., Tiwary, A. K., & Singh, S. (2023). Experimental investigation on the performance of ground granulated blast furnace slag and nano-silica blended concrete exposed to elevated temperature. *Construction and Building Materials, 394*, 132088. https://doi.org/10.1016/j.conbuildmat.2023.132088

Tanyildizi, H., & Coskun, A. (2008). The effect of high temperature on compressive strength and splitting tensile strength of structural lightweight concrete containing fly ash. *Construction and Building Materials, 22*(11), 2269–2275. https://doi.org/10.1016/j.conbuildmat.2007.07.033

Tao, Z., & Yu, Q. (2012). Residual bond strength in steel reinforced concrete columns after fire exposure. *Fire Safety Journal, 53*, 19–27. https://doi.org/10.1016/j.firesaf.2012.06.010

Zhang, H. Y., Kodur, V., Wu, B., Cao, L., & Qi, S. L. (2015). Effect of carbon fibers on thermal and mechanical properties of metakaolin fly-ash-based geopolymers. *ACI Materials Journal*. https://doi.org/10.14359/51687391

Zhang, Y., Yuan, Z., Zhang, L., Zhang, X., Ji, K., Ni, W., & Wang, L. (2025). Experimental and theoretical study of fire resistance of steel slag powder concrete beams. *Engineering Structures, 325*, 119402. https://doi.org/10.1016/j.engstruct.2024.119402

Publisher's Note